Article

Not peer-reviewed version

Multi-Platform LiDAR Comparative Assessment for Above-Ground Biomass and Carbon Estimation in Mediterranean Woody Crops

Mateo Pastrana *, Cristina Velilla-Lucini, Nelson Mattié, Alfonso Gomez, Sergio Molina

Posted Date: 17 April 2026

doi: 10.20944/preprints202603.0280.v2

Keywords: laser scanning; olive; almond; aboveground biomass; carbon accounting; machine learning

 doi:10.20944/preprints202603.0280.v2

Article

Multi-Platform LiDAR Comparative Assessment for Above-Ground Biomass and Carbon Estimation in Mediterranean Woody Crops

Mateo Pastrana [1,*], Cristina Velilla-Lucini [1], Nelson Mattié [2], Alfonso Gomez [1,3] and Sergio Molina [4]

[1] School of Agricultural, Food and Biosystems Engineering, Universidad Politécnica de Madrid, Avda. Puerta de Hierro 2, 28040 Madrid, Spain.
[2] Alberta Centre for Earth Observation Sciences, Department of Earth and Atmospheric Sciences, University of Alberta, Edmonton, AB, T6G 2E3, Canada.
[3] Stereocarto Iberoamérica S.L., Carretera de Canillas 134, 28043. Madrid, Spain. agomez@stereocarto.com
[4] University of Jaén (UJA), Campus Las Lagunillas s/n, 23071 Jaén, Spain.
* Correspondence: mateo.pastrana@alumnos.upm.es

Highlights

What are the main findings?

- Four LiDAR modalities (PNOA/ALS, Riegl ALS, ULS, and MLS) were benchmarked for plot-scale and tree-scale AGB and carbon estimations in Mediterranean woody crops.
- Species-specific allometry and fixed-area plot sampling enabled consistent biomass/carbon computations across the three farms in Córdoba (Spain).

What are the implications of the main findings?

- The National Aerial Orthophotography Plan (PNOA) can support scalable Measurement, Reporting, and Verification (MRV) workflows for orchard carbon monitoring under specific canopy and terrain conditions.
- Cross-platform harmonization and transparent validation are essential for defensible and reproducible estimates.

Abstract

Reliable Aboveground Biomass (AGB) estimates for woody crops are essential for carbon accounting and for Measurement, Reporting and Verification (MRV) frameworks. However, it remains unclear how LiDAR modality and sampling geometry influence plot-scale and tree-scale AGB predictions in intensively managed Mediterranean orchards. In this study, we benchmarked four LiDAR modalities, namely open national airborne laser scanning from the Spanish National Aerial Orthophotography Plan (PNOA/ALS), a dedicated Riegl airborne laser scanner (ALS), unmanned laser scanning (ULS) and mobile laser scanning (MLS), across three woody-crop sites in Córdoba (southern Spain): IFAPA, Doña María, and Villaseca. Plot-level LiDAR metrics (mean height, 95th height percentile, maximum height, and canopy cover proxies) were extracted from normalised point clouds and related to field AGB using Random Forest and XGBoost regression models, together with an ensemble predictor, under an 80/20 train–test split. In parallel, TreeQSM-based Quantitative Structure Models (QSMs) were evaluated as an independent tree-level three-dimensional reconstruction approach. XGBoost achieved the lowest errors at IFAPA (RMSE = 0.400 Mg ha^{-1}; R^2 = 0.994) and Villaseca (RMSE = 0.872 Mg ha^{-1}; R^2 = 0.995), whereas PNOA/ALS was competitive at Doña María (RMSE = 0.725 Mg ha^{-1}; R^2 = 0.994). TreeQSM closely matched field inventory at the low-biomass IFAPA site but tended to overestimate biomass at Doña María and Villaseca, and only 28% of scanned trees yielded usable reconstructions. The results support the use of cross-platform LiDAR for orchard AGB and carbon mapping and identify the conditions under which open national LiDAR can enable scalable MRV of Mediterranean woody crops.

 doi:10.20944/preprints202603.0280.v2

Keywords: laser scanning; olive; almond; aboveground biomass; carbon accounting; machine learning

1. Introduction

Woody-crop agroecosystems such as olive and almond orchards store substantial amounts of carbon in long-lived woody biomass and are increasingly relevant for carbon accounting and for Measurement, Reporting and Verification (MRV) frameworks in agriculture. Field inventories remain the benchmark for Aboveground Biomass (AGB) estimation, but they are labour-intensive and difficult to repeat at operational scales. Light Detection and Ranging (LiDAR) provides three-dimensional structural measurements that enable robust plot-scale AGB modelling, typically by relating plot metrics derived from height distributions and canopy cover proxies to field-derived AGB through area-based approaches [1,2].

Orchards differ from natural forests in canopy architecture, with low-to-moderate stature, row-based planting patterns, and structures that are strongly shaped by management. These features can amplify scan-geometry effects such as occlusion and non-uniform sampling. In Mediterranean olive systems, airborne LiDAR has demonstrated its utility for structural estimation and for biomass-related proxies [3,4], while orchard carbon assessments have highlighted the strong dependence of carbon sequestration on planting intensity and management practices [5]. At broader scales, spaceborne LiDAR missions such as the Global Ecosystem Dynamics Investigation (GEDI) have further reinforced the value of structural observations for biomass monitoring over large areas [6,7], although their footprint size and sampling design make them unsuitable for the characterization of individual orchards and therefore motivate the use of higher-resolution airborne, unmanned, and mobile LiDAR systems in this context.

A growing body of literature has explored multi-platform LiDAR for AGB estimation. Airborne laser scanning (ALS) has been widely used as a reference for area-based AGB modelling in forests and, more recently, in woody crops [1–3,8]. Unmanned laser scanning (ULS) has gained attention because of its very high point density and operational flexibility, enabling detailed crown reconstruction over small plots and farms. Mobile and terrestrial laser scanning (MLS and TLS) provide close-range, very dense point clouds that support individual-tree reconstructions and Quantitative Structure Modelling (QSM) [9]. Studies combining two or more LiDAR platforms have shown that differences in point density, scan geometry, and multi-return structure can introduce systematic offsets in height percentiles and canopy cover metrics, with direct consequences for plot-scale AGB estimates. However, most existing multi-platform comparisons have been carried out in natural forests or plantations with more vertically developed canopies; systematic benchmarking across airborne, unmanned, and mobile LiDAR in low-to-moderate stature Mediterranean woody crops remains scarce.

A key operational question for MRV is how much LiDAR detail is actually required for reliable AGB estimation. Open national airborne LiDAR program, such as Spain's PNOA-LiDAR [18], provide broad, repeated coverage at relatively low point densities, whereas dedicated ALS, ULS, and MLS surveys provide denser sampling with distinct geometries but also introduce potential occlusion and strip-alignment artefacts [8,9]. As a consequence, cross-platform benchmarking of Mediterranean woody crops is still limited, and it remains unclear to what extent open national LiDAR can match the performance of dedicated airborne, unmanned, and mobile acquisitions for orchard-scale AGB and carbon estimation.

In this context, the main objective of the present study was to compare plot-scale AGB estimation accuracy obtained from four LiDAR modalities (PNOA/ALS, Riegl ALS, ULS, and MLS) in Mediterranean woody crops, and to assess the conditions under which open national LiDAR is competitive with dedicated airborne, unmanned, and mobile LiDAR acquisitions. To achieve this, we established 58 fixed-area plots (1,867 trees) across three woody-crop sites in Córdoba (southern Spain) and used species-specific allometries together with machine-learning regression models, namely

 doi:10.20944/preprints202603.0280.v2

Random Forest and XGBoost [10,11], to predict plot-scale AGB and carbon from LiDAR metrics. In parallel, and in a complementary line of analysis, we evaluated TreeQSM-based Quantitative Structure Models as an independent tree-level three-dimensional reconstruction approach, in order to assess when and where geometric reconstruction can add value to area-based predictors in orchard MRV applications.

Beyond area-based plot metrics, an increasingly important line of work leverages quantitative structural models (QSMs) to reconstruct tree geometries directly from 3D point clouds. QSM approaches, typically based on fitting cylinder primitives to woody skeletons, aim to estimate stem/branch volume and related structural attributes at the individual-tree level, enabling biomass inference with a more explicit geometric basis than summary height or density metrics. In principle, QSM-derived descriptors can reduce reliance on purely empirical relationships and improve transferability across sites when point density and occlusion conditions allow faithful reconstruction. However, QSM performance is highly sensitive to point-cloud quality and sampling geometry: noise, variable point density, occlusion, and segmentation errors can propagate into biased volume estimates, especially in complex crowns, hedgerow architectures, and intensively managed orchards where canopy structure departs from typical forest forms. Consequently, the feasibility and reliability of QSMs in woody-crop settings remain less established than those in forest terrestrial laser scanning (TLS) applications, and systematic comparisons against conventional inventory-based allometry and plot-level LiDAR models are still limited.

Therefore, in this study, we complemented cross-platform plot-scale modeling with a TreeQSM-based QSM evaluation as an independent, tree-level 3D reconstruction pathway. By comparing QSM-derived biomass estimates with field inventory across sites spanning low- to higher-biomass conditions, we assessed not only accuracy but also practical usability (e.g., proportion of trees successfully reconstructed) under real acquisition constraints. This dual perspective of geometric reconstruction (QSM) versus area-based predictors (ML models) helps clarify when 3D structural modeling offers added value for biomass and carbon estimation in Mediterranean woody-crop agroecosystems.

2. Materials and Methods

2.1. Study Sites

The study was conducted in three farms in the province of Córdoba (southern Spain): IFAPA (Finca Experimental de la Alameda del Obispo, Córdoba, Spain), Doña María (Córdoba, Spain; Cerro del Obispo, S.L.), and Villaseca (Almodóvar del Río, Córdoba, Spain; Agrícola Villaseca S.L., Cortijo La Reina). The sites span research to commercial settings and contrasting orchard structures (Figure 1).

IFAPA: The study area covers approximately 6.82 ha within the Alameda del Obispo experimental farm, a research station operated by IFAPA and co-located with CSIC and INIA facilities. The study focused on olive and almond plots with the following planting layouts: olive 6×2.5 m, 4×1.5 m and 7×3.4 m; almond 7×6 m, 3.5×1.2 m and 6×3 m. The site shows predominantly flat terrain with very gentle slopes and an altitude ranging from approximately 100 to 120 m above sea level. Soils are alluvial with sandy-loam texture and substantial silt content, and soil depth exceeds 2 m. The climate is Mediterranean, with a mean annual precipitation of approximately 600 mm concentrated between October and April. For the 2024 reference year, the mean annual temperature was 19°C, annual precipitation 572 mm and mean relative humidity (RH) 64%; prevailing winds blow from east to west. The site is located in the Guadalquivir floodplain, where flood risk is relevant. Olive and almond orchards were established in 2018, with drip irrigation, manual and mechanical pruning, olive harvest in November–December and almond harvest in August.

Doña María: Topographically variable farm combining new plantings with older trees; 3 parcels defined for analysis. The farm is described as 187 ha (farm description) and 261.45 ha (spatial data extent). Olive (Olea europaea) with Picual and Arbequina varieties. Square-shaped with undulating relief; mean slope 2.7%; altitude ~230 m a.s.l.; clay soil (other chemical properties not available). Mean

Preprints.org (www.preprints.org) | NOT PEER-REVIEWED | Posted: 17 April 2026 doi:10.20944/preprints202603.0280.v2

annual temperature ~19°C; precipitation ~600 mm; RH ~65%; prevailing winds W→E; groundwater resources mentioned. Drip irrigation; mineral fertilization; manual pruning; chemical pest control; olive harvest November-December.

Villaseca: Commercial, intensively managed farm; 13 parcels derived for analysis and scalability testing. The total farm area is ~85 ha. Regular square shape and flat relief; slope 1.80%; altitude ~80 m a.s.l.; orientation NW–SE; clay-loam soil, depth ~2 m; pH 8.5; organic matter 1.20%. For 2024: mean temperature 18.5°C, precipitation 697 mm, RH 65%; prevailing winds W→E. Olive and almond planting established in 2018; drip irrigation; fertilization with liquid mineral fertilizers; phytosanitary treatments applied.

Figure 1. Location of the study sites.

2.2. *Field Inventory, Plot Design, and Biomass/Carbon Computation*

Fixed-area rectangular plots of 20 m × 50 m (1000 m²; 0.1 ha) were used as the primary sampling units (Figure 2). Plots were selected using simple random sampling to minimize selection bias and ensure independence among observations. A total of 58 plots were surveyed (Doña María: 18; IFAPA: 20; Villaseca: 20). Field measurements were collected during December 2024 and January 2025 across three farms (Villaseca, Doña María, and IFAPA). Tree diameters were measured with a measuring tape, and tree height was measured (Figure 3) using two 5 m extendable poles (calibrated prior to measurements). Plot locations were handled using a mobile GNSS application (GPS Fields Area Measure) and photo documentation, and the data were recorded using standardized spreadsheets.

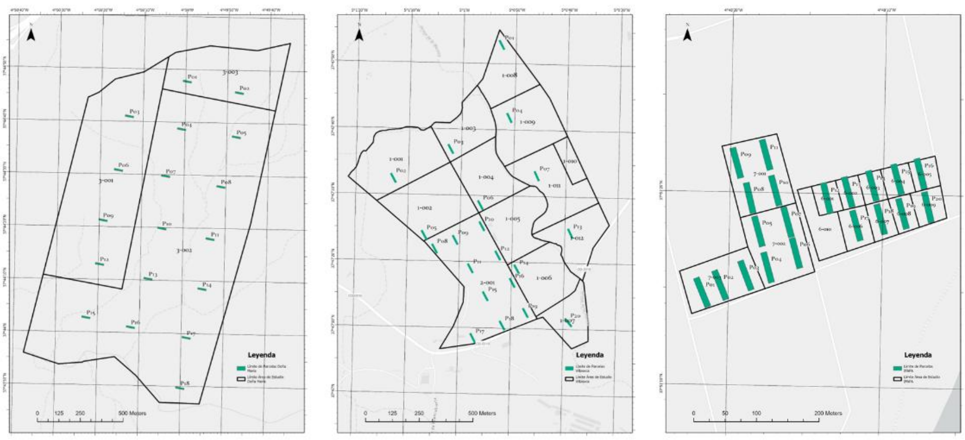

Figure 2. Study sites and field inventory plots.

Preprints.org (www.preprints.org) | NOT PEER-REVIEWED | Posted: 17 April 2026 doi:10.20944/preprints202603.0280.v2

Figure 3. a. Methodology and equipment used for field measurements.

Figure 3. b. Methodology and equipment used for field measurements.

Tree-level aboveground biomass (AGB, kg dry matter) was computed using component-wise allometric equations parameterized by the trunk diameter below the first bifurcation (D2r, cm).

For almond (Prunus dulcis), component biomass was computed as:

- Branches: $B_{branches} = 0.0688 \times D2r^{2.2061} \times 1.1349 \times \varrho$;
- Stem: $B_{stem} = 0.3346 \times D2r^{1.9656} \times 0.9968 \times \varrho$;
- Foliage: $B_{foliage} = 0.0165 \times D2r^{1.3212} \times 0.9564 \times \varrho$.

For olive (Olea europaea), component biomass was computed as:

- Branches: $B_{branches} = 0.251 \times D2r^{2.071} \times \varrho$;
- Stem: $B_{stem} = 0.0785 \times D2r^{2.527} \times \varrho$;
- Foliage: $B_{foliage} = 0.0446 \times D2r^{1.724} \times \varrho$.

Wood density was set to $\varrho = 0.76\ g \cdot cm^{-3}$ for almond (Prunus dulcis) and $\varrho = 0.56\ g \cdot cm^{-3}$ for olive (Olea europaea). D2r was measured in cm; component biomass is in kg. The equations are applicable for 5-50 cm trunk diameter. The tree AGB was computed as the sum of the components. Plot-level AGB density ($Mg\ ha^{-1}$) was derived by summing the tree AGB within each plot, converting kg to Mg, and dividing by the plot area (0.1 ha).

Tree-level AGB (kg) was converted to carbon (C, kg C) using mean wood carbon fractions of 44.5% for olives and 45.7% for almonds ($C_{Olive} = AGB \times 0.445$; $C_{Almond} = AGB \times 0.457$). CO2-

equivalent was computed as CO2e = 3.67 × C following IPCC molecular-weight conversion. Carbon-fraction sources include orchards and olive allometry/carbon studies [4,5,12,13].

Table 1. Field inventory summary by site (mean ± standard deviation).

Site	Statistic	N_trees_plot	D2r_cm	Height_m	AGB_Mg_ha	C_Mg_ha
Villaseca	Mean	55.1	17.76	5.09	33.89	15.93
Villaseca	Std. Dev.	27.48	8.06	2.42	9.64	4.53
Doña María	Mean	18.44	17.12	4.18	30.94	14.54
Doña María	Std. Dev.	0.83	2.43	0.31	9.35	4.39
IFAPA	Mean	21.65	13.8	3.96	12.76	6
IFAPA	Std. Dev.	12.04	3.35	0.44	5.34	2.51

2.3. LiDAR Datasets

Four LiDAR modalities were analyzed in this study: (i) the Spanish National Aerial Orthophotography Plan LiDAR (PNOA/ALS), which is an open national airborne LiDAR program [18]; (ii) a dedicated airborne laser scanner (ALS) based on a RIEGL LMS-Q680i sensor; (iii) an unmanned laser scanning (ULS) system mounted on a DJI platform and equipped with a DJI Zenmuse L2 sensor; and (iv) a mobile laser scanning (MLS) system (LiDAR USA Snoopy A-Series with Velodyne HDL-32E). The Riegl ALS acquisition and associated flight plans are shown in Figure 4, while Figure 5 illustrates the corresponding PNOA/ALS point cloud data and cross-sections. The ULS DJI flight plans and classified point clouds are presented in Figure 6, and the MLS Snoopy terrestrial trajectories and point clouds are shown in Figures 7 and 8.

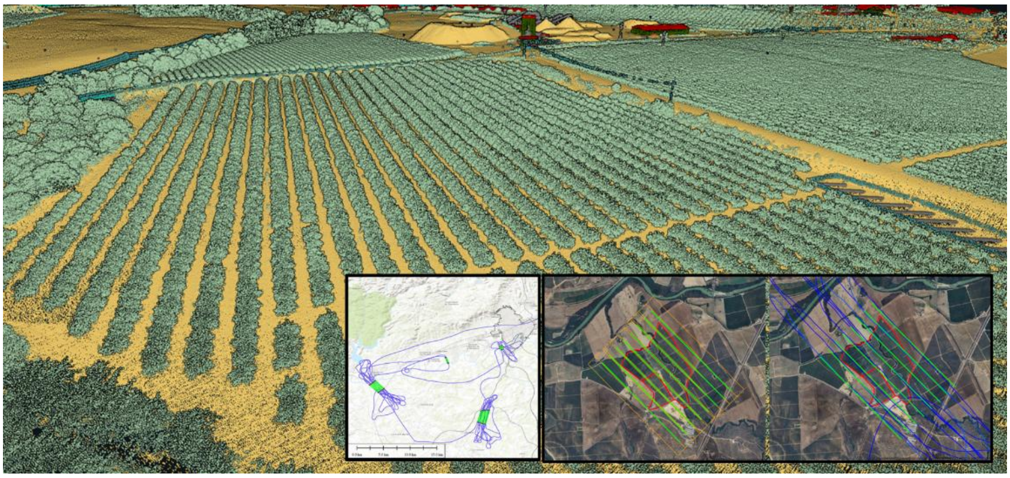

Figure 4. ALS Riegl airborne flight plans and classifies point cloud data.

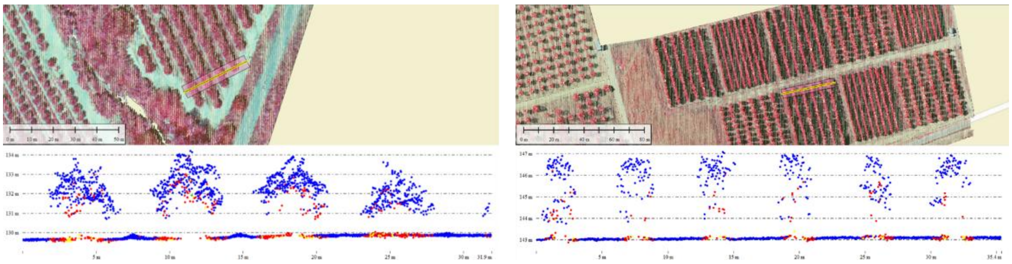

Figure 5. ALS PNOA point cloud data and cross sections.

Preprints.org (www.preprints.org) | NOT PEER-REVIEWED | Posted: 17 April 2026 doi:10.20944/preprints202603.0280.v2

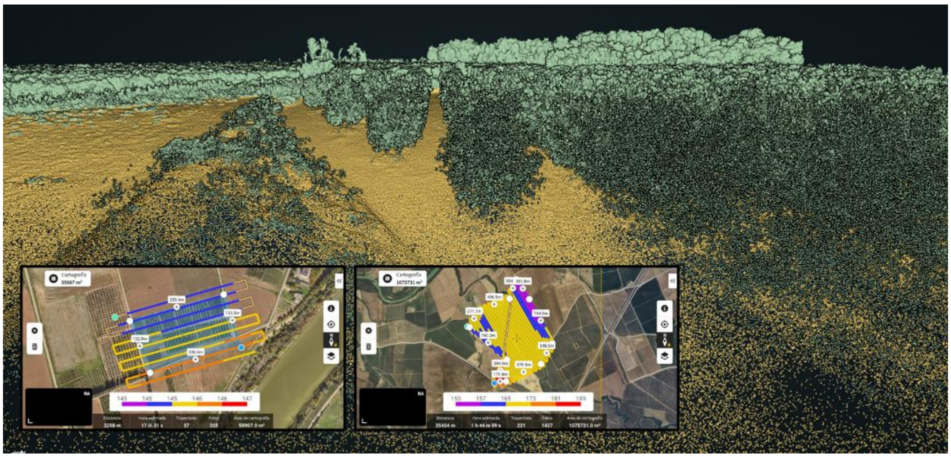

Figure 6. ULS DJI drone flight plans and classifies point cloud data.

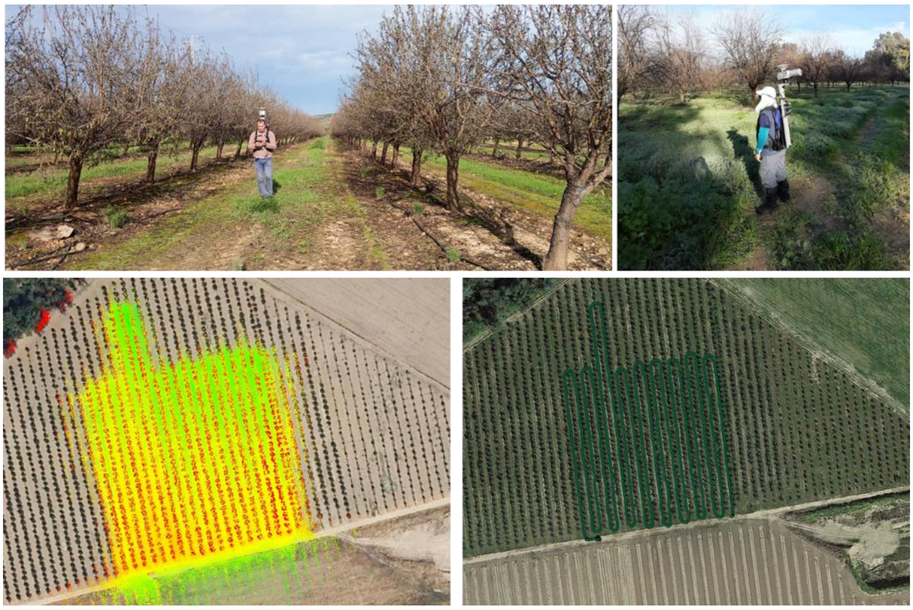

Figure 7. MLS Snoopy terrestrial trajectories and point cloud data.

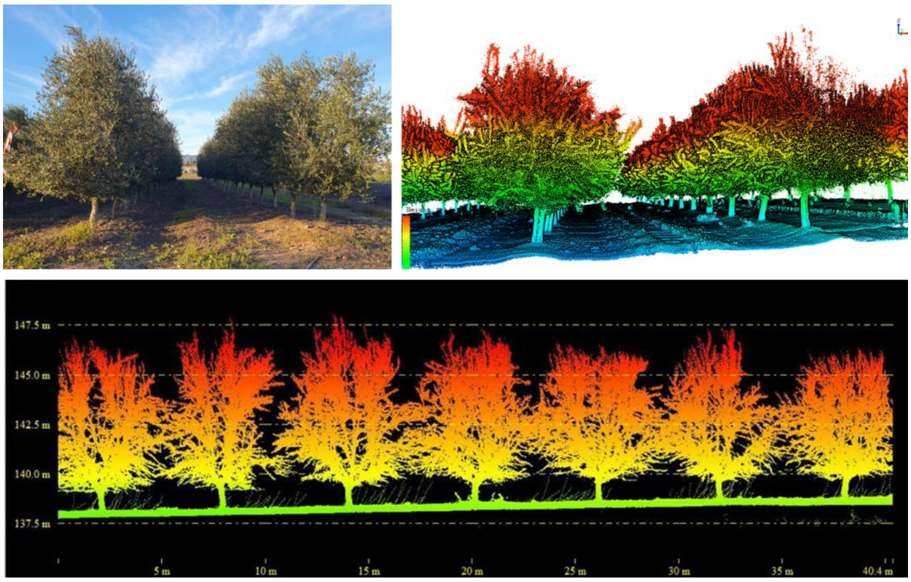

Figure 8. MLS Snoopy point cloud data.

Preprints.org (www.preprints.org) | NOT PEER-REVIEWED | Posted: 17 April 2026 doi:10.20944/preprints202603.0280.v2

ALS was prioritized for large extents (e.g., Doña María), ULS was used for detailed characterization in smaller areas (e.g., IFAPA), and MLS-supported close-range sampling was used (Figure 9). Dataset metadata, including point density and recommended CHM resolution, are summarized in Tables 2 and 3.

Table 2. LiDAR modality summary (density, suggested CHM resolution, and spatial reference metadata).

System	Point spacing (m)	Density (pts/m²)	Intensity (bits)	Color	Multiple returns	Scan angle (deg)	Flight/ Survey date	EPSG	Orthometric heights	Stated Accuracy XY/Z
PNOA ALS	0.447	5.0	16	RGBI	Yes (4)	-19.62 – 3.17°	27/09/2024	25830	EGM2008-REDNAP	0.30 / 0.10 m
Riegl ALS	0.146	46.8	8	RGB	Yes (7)	-30 – 30°	21/11/2024	32630	EVRS	0.06 / 0.06 m
ULS	0.02	2470.0	8	RGB	No	-35 – 35°	18/12/2024	32630	EVRS	0.10 / 0.05 m
MLS	0.005	36545.0	8	N/A	No	-90 – 65°	10/12/2024	32630	EVRS	0.02 / 0.02 m

Table 3. Sensor/platform and acquisition specifications (as provided).

	PNOA/ALS (national)	Riegl ALS	ULS	MLS
LiDAR system	Optech T2000	Riegl LMS-Q680i	DJI Zenmuse L2	LiDAR USA Velodyne hdl-32e
GNSS/IMU system	POS AV™ AP60 (OEM)	IGI IMU LIE	DJI 200 Hz	Snoopy INS (OEM)
Planning/navigation/post-processing software	Optech FMS y LMS (LiDAR Mapping Suite)	IGI Plan v1.5.5 /Aerocontrol/ Inertial Explorer 8.9 y AeroOffice 5.58	DJI Terra	Scan look PC LiDAR 360 Inertial explorer
Flight height (m)	2.200	420	80	2
FOV	50	60	70	40ºV – 360ºHZ
Scan frequency (Hz)		400		
Pulse frequency (kHz)	700-1.100	266	240	1.200
Speed	160 Knot	85 Knot	6 m/s	1 m/s
Nominal density (pts/m²)	5	11	300	33.000
FWF	Yes, not available	Yes	No	No
Returns	4	7	3	1
Intensity	16	8	8	8
Color	RGBI	ND	RGB	ND
Cross-track overlap	>15%	>90%	>90%	N/A
Reference system	IGN/RAP	IGN/RAP (CRBD)	IGN/RAP	IGN/RAP
Accuracy (XY/Z, m)	0,30/0,10	0,06/0,06	0,10/0,05	0,02/0,02

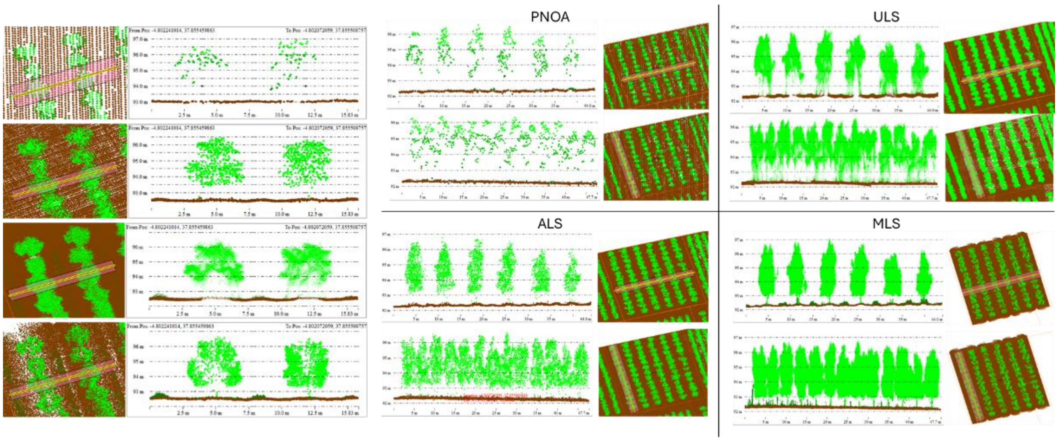

Figure 9. LiDAR point cloud data; cross-sections from all sensors.

2.4. Pre-Processing and Metric Extraction

LiDAR point clouds were processed to support cross-platform comparison. Pre-processing included noise filtering and outlier removal, ground/vegetation separation, point cloud classification and segmentation using deep learning algorithms, terrain interpolation to produce a digital terrain model (DTM), and height normalization to express point elevations relative to the ground. Canopy

 doi:10.20944/preprints202603.0280.v2

height models (CHMs) were generated by rasterizing normalized heights; pit-free CHM approaches can reduce canopy surface artifacts in discrete-return LiDAR [8].

For metric extraction, LAS/LAZ files were handled programmatically (e.g., using Laspy in Python and LasCanopy from LAStools), and plot-level structural metrics were computed from normalized point clouds. The project workflow describes plot metrics stored in CSV files per site and system, including mean height, 95th percentile of height (p95), maximum height, and canopy-cover proxies. Additional geometric descriptors (e.g., point density and slope/curvature metrics) were considered during preprocessing to characterize terrain and sampling effects.

Because sources differ in coordinate reference systems and orthometric height references, all datasets should be harmonized to a common horizontal CRS and vertical datum prior to comparison. The final submission should document the transformation parameters and quantify the residual co-registration errors.

2.5. Modeling and Validation

For each plot and each LiDAR system (PNOA/ALS, Riegl ALS, ULS, and MLS), plot-level structural metrics were extracted from the normalized point clouds and stored in per-system CSV tables. The extracted metrics included mean, maximum, and standard deviation of height, height percentiles such as the 25th, 50th, 75th, 90th, 95th and 99th percentiles (hereafter referred to as Relative Height metrics, RH25, RH50, RH75, RH90, RH95, and RH99, in analogy with the nomenclature commonly used for spaceborne and airborne LiDAR), several canopy-cover proxies (fraction of first returns above defined height thresholds, and Fractional Canopy Cover, FCC) and additional density and vertical variability descriptors. The field AGB (response variable) and the LiDAR metrics (predictors) were merged using a unique plot identifier. Non-predictive identifiers (e.g., plot ID, site labels) were removed before modelling, and all remaining predictors were standardized using a z-score scaler (StandardScaler from scikit-learn) to ensure comparable scales across variables and LiDAR systems. Two machine-learning regressors were trained for each LiDAR system: a Random Forest Regressor [10] and an XGBoost Regressor [11]. Random Forest models were fitted with 500 trees and default scikit-learn hyper-parameters, using the mean squared error as the splitting criterion and the out-of-bag samples for internal error estimation. XGBoost models were trained with a learning rate of 0.05, a maximum tree depth of 6, and 500 boosting rounds, using the squared error objective. For each LiDAR system an ensemble prediction was also computed as the arithmetic mean of the Random Forest and XGBoost predictions, in order to explore whether combining the two regressors reduced residual variance. Feature importance was examined using the built-in Gini-based importance for Random Forest and gain-based importance for XGBoost, which provided additional insight into which structural metrics contributed most to plot-scale AGB prediction for each LiDAR modality.

The data were split into training and test subsets using an 80/20 random partition, stratified by site, in order to assess the generalization capacity of the models on unseen plots. Model performance was reported using the coefficient of determination (R^2), the Root Mean Squared Error (RMSE), the Mean Absolute Error (MAE), and the absolute and relative bias, computed both on the test set and on the full dataset. Villaseca and Doña María were primarily used for model development and internal testing, while IFAPA was additionally used as an external validation site to assess the transferability of the models to a contrasting orchard and climatic configuration.

To compare structural variables and derived biomass and carbon estimates among sites and LiDAR systems, a formal statistical testing workflow was designed. First, the normality of each variable was assessed with the Shapiro–Wilk test, and the homogeneity of variances was tested using Levene's test. Second, when the assumptions of normality and homoscedasticity were met, a one-way Analysis of Variance (ANOVA) was applied to test for differences in mean values among sites and/or LiDAR systems. Third, when these assumptions were not met, the non-parametric Kruskal–Wallis test was used as an alternative to compare the distribution of ranks across groups. Dunn's post-hoc test with Bonferroni correction was subsequently applied to the Kruskal–Wallis significant cases in order to identify the specific group pairs driving the differences. The significance level was

Preprints.org (www.preprints.org) | NOT PEER-REVIEWED | Posted: 17 April 2026 doi:10.20944/preprints202603.0280.v2

set at α = 0.05 throughout the analysis. This combined parametric and non-parametric framework ensured that the site and platform comparisons reported in the Results section were statistically robust irrespective of the underlying distributional assumptions.

In addition to the plot-level area-based models, we evaluated a tree-level 3D reconstruction approach using TreeQSM (Figures 10 and 11). In our workflow, TreeQSM was applied to point clouds generated only by MLS, in which individual-tree subsets could be isolated with sufficient quality (i.e., adequate point density, limited noise, and reduced occlusion). Prior to the QSM reconstruction, point clouds were filtered to remove outliers and non-woody points, and tree-level subsets were extracted using the available segmentation outputs and field plot information. QSM outputs were inspected for geometric plausibility (e.g., continuous branching structure and realistic cylinder radii) and flagged when reconstruction artifacts indicated segmentation failure or insufficient sampling.

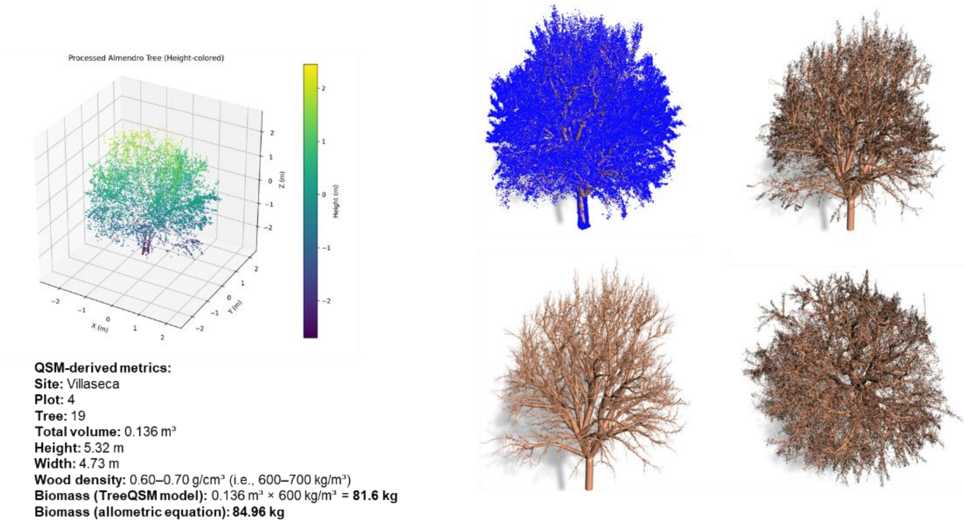

Figure 10. QSM Reconstructed 3D model of the almond tree.

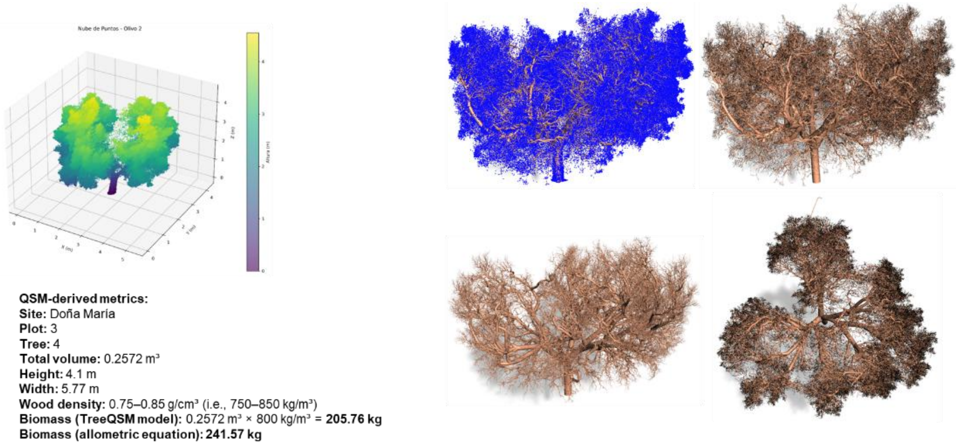

Figure 11. QSM Reconstructed 3D model of the olive tree.

TreeQSM-derived woody volume estimates were converted to biomass using species-appropriate wood density values and, where required, converted to carbon and CO_2-equivalent using the same carbon fractions and CO_2 conversion factor applied to inventory-derived estimates to ensure comparability. The QSM pathway is conceptually distinct from the area-based approach: rather than predicting plot AGB from summary LiDAR metrics, QSM estimates are grounded in the explicit reconstruction of 3D tree geometry. This provides a complementary line of evidence to assess

Preprints.org (www.preprints.org) | NOT PEER-REVIEWED | Posted: 17 April 2026 doi:10.20944/preprints202603.0280.v2

whether geometric reconstruction can reduce bias relative to purely empirical predictors, particularly across sites with contrasting orchard architectures.

Because QSM performance is strongly dependent on point cloud completeness and density, we quantified practical usability by reporting the proportion of trees for which TreeQSM produced usable reconstructions. Reconstructions were considered usable only when (i) the fitted model represented a coherent woody structure and (ii) key structural attributes were within plausible ranges for the species and management system. Trees were excluded when the reconstruction was compromised by insufficient point density, excessive noise, severe occlusion, or segmentation errors. This usability metric is critical for operational deployment because QSM methods can deliver high-fidelity outputs only for a subset of trees under typical orchard acquisition conditions.

TreeQSM-derived biomass estimates were evaluated against field inventory at the tree level using standard regression diagnostics and error metrics, including the coefficient of determination (R^2), bias, and dispersion of residuals. When appropriate, the results were summarized by site to test for site-dependent agreement and systematic over- or underestimation patterns. In parallel with the machine-learning models, we emphasize that QSM–inventory agreement should be interpreted in light of sampling geometry and data quality constraints; therefore, we report both accuracy metrics and the fraction of trees successfully reconstructed as complementary indicators of performance and applicability.

3. Results

3.1. Field Biomass and Carbon Stocks

The field inventory indicated strong site differences in structure and biomass (Table 1). Mean AGB was 33.89 Mg ha−1 in Villaseca, 30.94 Mg ha−1 in Doña María, and 12.76 Mg ha−1 in IFAPA (Figures 12a, 12b and 12c). These contrasts are consistent with the differences in planting layout, management, and site conditions described in Section 2.1.

Figure 12. a. Villaseca site, biomass estimations per site per plot.

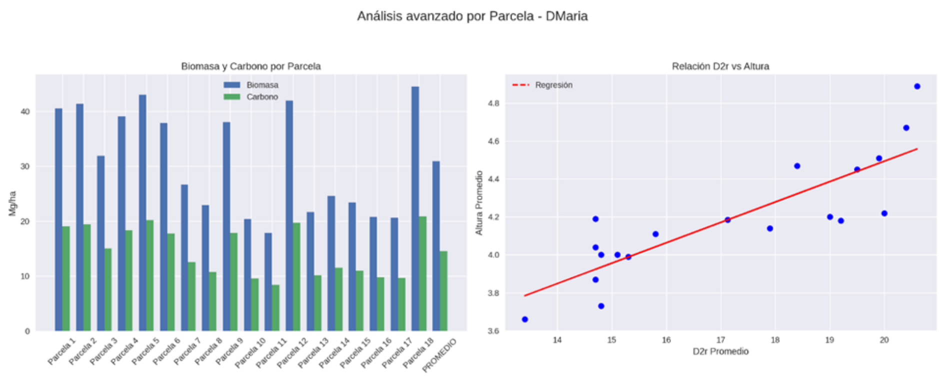

Figure 12. b. Doña Maria site, biomass estimations per site per plot.

 doi:10.20944/preprints202603.0280.v2

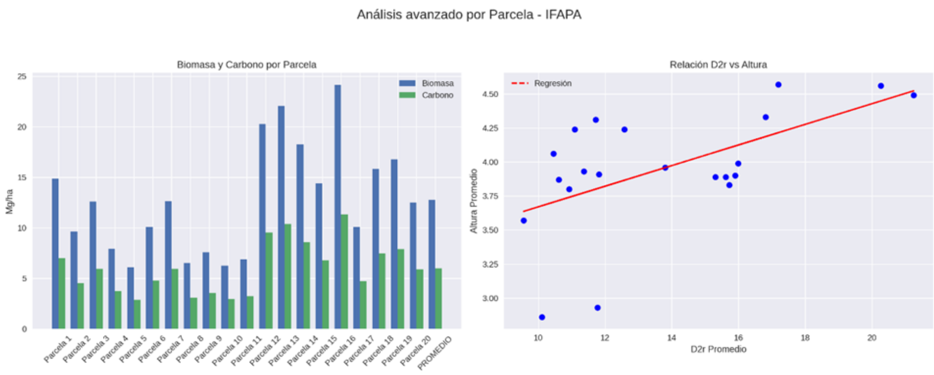

Figure 12. c. IFAPA site, biomass estimations per site per plot.

3.2. Model Performance

The performance of the plot-scale AGB models obtained for each site and LiDAR modality is summarized in Table 5 and illustrated in Figures 13, 14, and 15. Figure 13 shows the scatter plots of predicted versus observed plot AGB for each site and LiDAR system, Figure 14 presents the analysis of residuals, and Figure 15 shows the evolution of the biomass estimation error throughout the modelling process. Considering the cross-platform comparison carried out at Doña María, where ALS, PNOA/ALS, and MLS point clouds were all available for the same plots, the PNOA/ALS-based model achieved the best performance (RMSE = 0.725 Mg ha^{-1}, relative RMSE = 2.36%, R^2 = 0.994), closely followed by the Riegl ALS model (RMSE = 1.743 Mg ha^{-1}, R^2 = 0.985) and the MLS model (RMSE = 2.168 Mg ha^{-1}, R^2 = 0.988). At IFAPA and Villaseca, the comparison focused on the performance of the Random Forest, XGBoost, and ensemble regressors trained on the best-performing LiDAR configuration available for each site. At IFAPA, XGBoost clearly outperformed Random Forest and the ensemble, with RMSE decreasing from 1.542 Mg ha^{-1} (Random Forest) to 0.400 Mg ha^{-1} (XGBoost), and R^2 increasing from 0.932 to 0.994. A similar pattern was observed at Villaseca, where XGBoost achieved RMSE = 0.872 Mg ha^{-1} (R^2 = 0.995) compared with RMSE = 3.060 Mg ha^{-1} (R^2 = 0.950) for Random Forest. The ensemble predictor consistently reduced the errors of the Random Forest model but did not reach the accuracy of XGBoost. Overall, the cross-platform comparison indicates that, under the conditions of this study, the open national PNOA/ALS dataset can be competitive with much denser dedicated acquisitions for plot-scale AGB modelling in Mediterranean woody crops, provided that the regression models and the feature set are adapted to the lower point density of the PNOA/ALS data.

3.3. Cross-Site Comparison of Results

Statistical testing (ANOVA and Kruskal-Wallis) indicated that Villaseca, Doña María, and IFAPA differed significantly in D2r, tree height, trees per plot, biomass, carbon, and CO_2e, with consistently very low p-values. Doña María shows higher and more stable biomass and carbon stocks (small standard errors), suggesting relatively homogeneous growth conditions and management. In contrast, IFAPA exhibited greater dispersion, and the observed inverse D2r-biomass pattern indicates stronger environmental and/or management-driven variability within the site. Villaseca presents an intermediate and, in some metrics, a contrasting response relative to the other sites, making it particularly useful as a benchmark under differing structural and management conditions.

3.4. Statistical Comparison Across Sites (ANOVA and Kruskal–Wallis)

To assess whether tree structure and biomass-related variables differed among the three study sites (Villaseca, Doña María, and IFAPA), we applied both a parametric one-way analysis of variance (ANOVA) and a non-parametric Kruskal–Wallis test. The results are summarized in Table 4 and Figures 13, 14, and 15.

 doi:10.20944/preprints202603.0280.v2

ANOVA results. One-way ANOVA indicated statistically significant differences among the sites for most variables. Specifically, the mean D2r differed across sites (F ≈ 3.35, p = 0.0421), as did the mean tree height (F ≈ 3.51, p = 0.0365). The number of trees per plot showed a strong site effect (F = 27.28, p < 0.0001). Similarly, plot-level biomass density differed markedly among sites (F = 39.48, p < 0.0001), and the same strong site effect was observed for carbon density (F = 39.48, p < 0.0001). Collectively, these results suggest that differences in site conditions and management practices are associated with significant variations in orchard structure, productivity, and carbon stocks.

Kruskal–Wallis results. Because normality cannot always be assumed, we complemented the ANOVA with the Kruskal–Wallis test. The Kruskal–Wallis statistic for D2r suggested a trend toward site differences (H ≈ 5.34, p = 0.0694), although it was marginally non-significant at the conventional α = 0.05 level. For height, no significant differences were detected (H ≈ 2.34, p = 0.3104). In contrast, the number of trees per plot remained highly site-dependent (H ≈ 28.86, p < 0.0001), and both biomass density (H ≈ 37.97, p < 0.0001) and carbon density (H ≈ 37.97, p < 0.0001) exhibited strong consistent differences among sites.

Overall, the agreement between ANOVA and Kruskal–Wallis for tree density (N_trees), biomass, and carbon provides robust evidence that site-specific conditions and management exert a strong influence on these key variables, whereas differences in D2r and height appear to be weaker and more sensitive to distributional assumptions.

Table 4. Summary integrating the results of both tests: ANOVA and Kruskal-Wallis.

Variable	ANOVA: F-statistic (p-value)	Kruskal-Wallis: H-statistic (p-value)
D2r	3.35 (0.0421)	5.34 (0.0694)
Tree Height	3.51 (0.0365)	2.34 (0.3104)
N_Tree	27.28 (<0.0001)	28.86 (<0.0001)
Biomass	39.48 (<0.0001)	37.97 (<0.0001)
Carbon	39.48 (<0.0001)	37.97 (<0.0001)

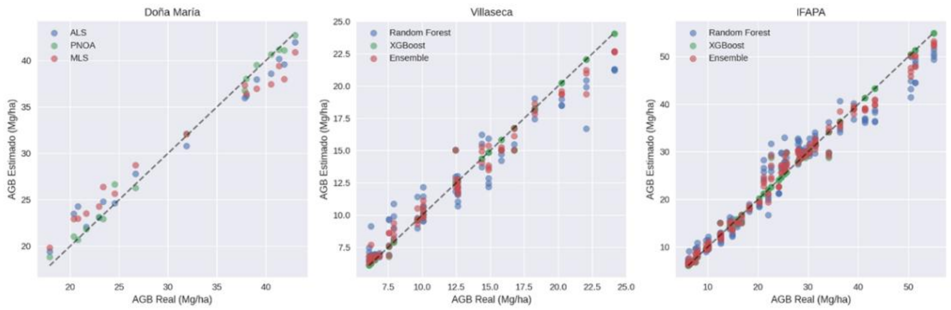

Figure 13. Scatter Plots.

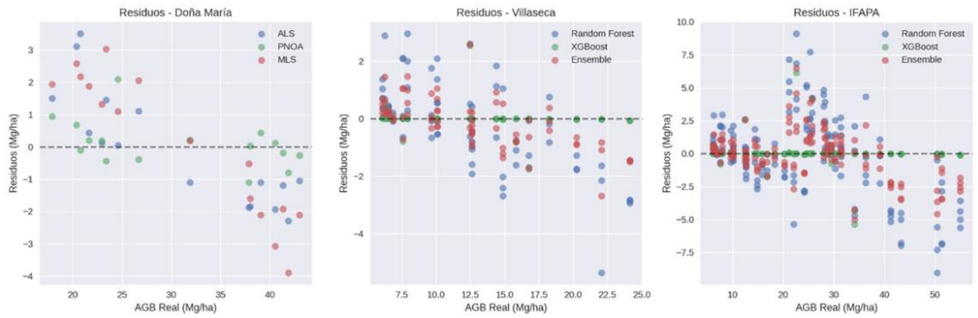

Figure 14. Analysis of Residuals.

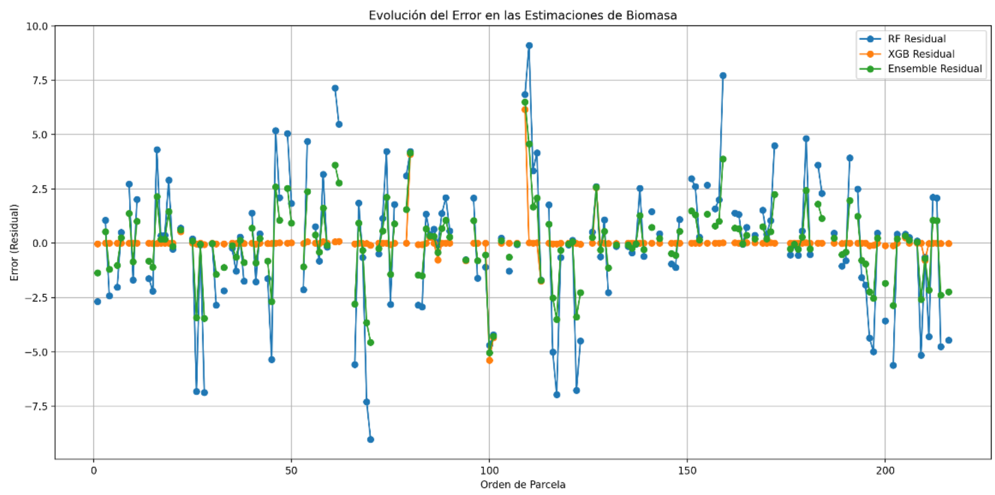

Figure 15. Biomass estimation error evolution.

Table 5. Model performance summaries extracted from project documentation.

Site	Group	RMSE_Mg_ha	Rel_RMSE_%	Bias_Mg_ha	Rel_Bias_%	R²	Mean_Rel_Error_%	SD_Rel_Error_%
Doña María (platform comparison)	ALS	1.743	5.671	-0.0675	-0.219	0.985	1.382	6.865
Doña María (platform comparison)	PNOA	0.725	2.359	0.1025	0.333	0.994	0.713	2.809
Doña María (platform comparison)	MLS	2.168	7.053	0.065	0.211	0.988	2.298	7.496
IFAPA (model comparison)	Random Forest	1.542	12.559	-0.182	-1.484	0.932	1.859	13.150
IFAPA (model comparison)	XGBoost	0.400	3.257	-0.003	-0.025	0.994	0.105	3.275
IFAPA (model comparison)	Ensemble	0.849	6.918	-0.092	-0.755	0.981	0.982	7.185
Villaseca (model comparison)	Random Forest	3.060	12.853	-0.010	-0.042	0.950	2.547	12.797
Villaseca (model comparison)	XGBoost	0.872	3.666	-0.004	-0.017	0.995	0.137	3.796
Villaseca (model comparison)	Ensemble	1.714	7.200	-0.007	-0.029	0.984	1.342	7.223

3.5. TreeQSM Tree-Level Reconstruction Results

The TreeQSM pathway was evaluated at the tree level using MLS point clouds as input. Of the 1,867 trees surveyed in the field across the three sites, only 522 trees yielded a usable TreeQSM reconstruction, corresponding to approximately 28% of the total. The remaining 72% were discarded because of insufficient point density, excessive noise, severe occlusion, or segmentation errors that compromised the geometric plausibility of the fitted models. This limited usability is a direct consequence of the orchard acquisition geometry, in which branches in the upper canopy can be poorly represented by MLS sweeps carried out between the rows.

For the subset of trees with usable reconstructions, TreeQSM-derived biomass was compared with field inventory estimates at the tree level. At the low-biomass IFAPA site, TreeQSM closely matched the field inventory, with a mean biomass of 51.14 kg tree^{-1} compared with 51.11 kg tree^{-1} from the inventory ($\Delta = 0.03$ kg tree^{-1}; $R^2 = 0.61$). In contrast, TreeQSM tended to overestimate biomass at Doña María and Villaseca by approximately +115.78 and +43.03 kg tree^{-1}, respectively, with R^2 values of 0.42 and 0.59. These results indicate a clear site-dependent bias, with TreeQSM performing best at the site with the simplest canopy architecture and lowest biomass per tree, and progressively deteriorating in the older and more structurally complex orchards at Doña María and Villaseca. Together with the low fraction of usable reconstructions, these results highlight the practical limitations of TreeQSM in operational orchard MRV and motivate the complementary use of plot-scale area-based models, which remained robust across sites.

4. Discussion

Taken together, the results reported in Section 3 show that plot-scale AGB can be accurately estimated from multi-platform LiDAR in Mediterranean woody crops, but that the performance of both area-based and geometric reconstruction approaches depends strongly on site conditions, sampling geometry, and data quality. Among the machine-learning approaches, XGBoost consistently outperformed Random Forest, with a substantially lower residual standard deviation (0.876 Mg ha^{-1} against 3.07 Mg ha^{-1}), while the ensemble predictor improved Random Forest performance in approximately 60% of the cases but did not surpass XGBoost. The cross-sensor comparison also revealed systematic offsets between LiDAR sources (for example, elevation offsets of about 1.23 m versus 0.68 m between ULS and ALS), which highlight the need for explicit cross-sensor calibration and harmonization prior to pooling metrics or transferring models. The limited usability of TreeQSM reconstructions (around 28% of the scanned trees) further indicates that, for typical orchard acquisition geometries, tree-level QSM cannot be used as a stand-alone inventory tool and is best interpreted as a complementary geometric pathway to area-based models. Where feasible, 3D structural reconstructions provide geometrically explicit inputs that can reduce the reliance on purely empirical relationships and can inform the design of new allometric models in orchards, but their operational value is currently conditioned by point density and occlusion.

By combining fixed-area plot inventories, species-specific allometries, and cross-platform LiDAR metrics, this study provides a consistent framework for accurate plot-scale AGB and carbon estimation in Mediterranean woody crops. The results indicate that open national LiDAR from PNOA can be competitive with much denser dedicated airborne, unmanned, and mobile acquisitions under certain canopy and terrain conditions, which supports its use in scalable MRV workflows. To ensure that these conclusions are defensible at the operational level, two methodological priorities were addressed in the revised analysis: the documentation of the coordinate reference systems and vertical datums used, together with the residual co-registration errors between LiDAR sources; and a transparent reporting of the validation design, including the 80/20 train–test split, the use of IFAPA as an independent validation site, and the consideration of potential spatial autocorrelation effects on plot-level errors.

4.1. Comparative Performance of LiDAR Modalities

Our results confirm that differences among LiDAR modalities influence not only point density and geometric precision, but also critically, the ability to characterize canopy three-dimensional structure, which ultimately governs aboveground biomass (AGB) estimation. MLS provided the finest spatial detail and most faithful representation of individual-tree structure, capturing crown architecture, intra-canopy gaps, and even trunk bases with high clarity. Its close-range sampling and very high point density (≈36,500 pts m^{-2}) largely compensated for the absence of multiple returns, making MLS a valuable "3D ground-truth" reference for calibrating structural metrics and validating other modalities.

ALS has emerged as the most balanced modality for operational biomass modeling, combining broad airborne coverage with multi-return capability (up to seven returns) and high vertical precision (≈0.06 m). This configuration enables robust retrieval of vertical canopy structures, including lower strata, which supports the modeling of height percentiles (e.g., RH metrics), canopy cover proxies (FCC), and height heterogeneity—features that are essential for plot-scale AGB estimation and regional upscaling.

Despite its exceptional point density (>2,000 pts m^{-2}), ULS exhibited limitations linked to inter-strip misalignments and the lack of multiple returns in some configurations, which can increase

 doi:10.20944/preprints202603.0280.v2

uncertainty in lower-canopy characterization. Nevertheless, ULS remains highly attractive for detailed sampling over limited extents owing to its operational agility and comparatively low cost, provided that geometric strip adjustment and radiometric/intensity harmonization are implemented.

The PNOA LiDAR (≈5–8 pts m^{-2}; up to four returns) provides a strong foundation for systematic mapping and long-term monitoring at large scales. Although its moderate density does not allow the canopy internal structure to be resolved with the same fidelity as ALS or MLS, its nationwide coverage and temporal consistency make it a key resource for repeated carbon monitoring and scalable inventory updates.

4.2. Implications for AGB Modeling

AGB modeling is strongly conditioned by the quality and characteristics of the input point clouds. In this study, metrics derived from ALS and PNOA, particularly height percentiles (e.g., RH50, RH95) and canopy cover fraction (FCC), showed stable relationships with field observations and supported allometric/regression models with relative errors typically below ~10–15% (site-dependent). For ULS and MLS, high-density and close-range sampling enable precise characterization of crown volume proxies and, in principle, tree-level biomass estimation; however, these modalities require modality-specific calibration and normalization to account for scan-angle effects, occlusion, and radiometric discrepancies among systems.

A key methodological issue is that the absence of multiple returns (or an inconsistent return structure) in the ULS and MLS can introduce positive bias in height-based percentiles, particularly when lower-canopy penetration is limited. This bias can be reduced through cross-modal fusion with ALS (multi-return reference), pass-level classification strategies, or harmonized point-cloud normalization workflows that explicitly model sampling completeness. Overall, our findings reinforce the value of LiDAR-derived structural metrics, especially RH metrics, height variance, and FCC, as robust predictors for biomass estimation in Mediterranean woody crops, consistent with prior evidence.

4.3. Scalability and Hierarchical Integration Strategy

A hierarchical integration of LiDAR modalities MLS, ALS, and PNOA has emerged as an effective and scalable framework for biomass and carbon estimation across spatial scales. Under this strategy, the MLS functions as a high-resolution 3D reference dataset to calibrate structural metrics, develop geometry-driven relationships, and validate local predictions. ALS then enables regional upscaling of these relationships, leveraging its intermediate density, strong vertical accuracy, and multi-return structure to capture vertical canopy variability over larger extents. Finally, PNOA LiDAR provides a pathway to extend AGB models to national-scale carbon inventories and long-term monitoring, benefiting from consistent coverage and repeat acquisitions.

This tiered approach optimizes acquisition costs by reserving ultra-dense surveys for calibration/benchmarking while using airborne sources for regional mapping and national programs for periodic updates. Importantly, it also strengthens the coherence between local observations and regional products, supporting reproducible methodologies for biomass and carbon quantification in woody-crop systems.

4.4. Limitations and Future Perspectives

The main limitations identified were (i) the limited number of vertical control points for rigorous cross-system vertical harmonization, (ii) the absence or inconsistency of multiple returns for some sensors/configurations, and (iii) radiometric/intensity discrepancies among systems. Future work should prioritize intensity normalization and radiometric harmonization algorithms, AI-based segmentation methods tailored to orchard architectures (including hedgerow systems), and multitemporal analyses using successive PNOA LiDAR acquisitions to quantify canopy growth dynamics and carbon accumulation over time.

 doi:10.20944/preprints202603.0280.v2

In addition, integrating LiDAR with high-resolution spectral imagery (multispectral or hyperspectral) is expected to improve biomass and productivity estimates by combining structural information with canopy conditions and vigor signals. Such multi-sensor fusion is particularly promising for woody agricultural systems, where management practices can decouple the structure from physiological status across seasons.

4.5. Comparison with Previous Studies

The plot-scale AGB accuracies obtained in this study are in line with, and in several cases improve upon, those reported by previous LiDAR-based studies in Mediterranean olive and almond orchards. Estornell et al. [3] combined airborne discrete-return LiDAR with field measurements to estimate wood volume and height in olive plantations in eastern Spain, reporting strong linear relationships between LiDAR-derived height and canopy metrics and field observations, with R^2 values typically in the range of 0.7–0.9. Velázquez-Martí et al. [4] developed dendrometric and wood-biomass allometries for Mediterranean olive orchards and highlighted the strong dependence of biomass on trunk diameter and basal area, which is consistent with the key role played by the diameter below the first bifurcation (D2r) in the present work. López-Bellido et al. [5] and Proietti et al. [16] quantified carbon sequestration in olive groves in southern Spain and Italy, respectively, and reported carbon densities broadly consistent with those obtained here from the field inventory, while also emphasizing that planting density, management intensity, and age strongly modulate orchard carbon stocks. In our dataset, the much lower field AGB observed at IFAPA (12.76 Mg ha^{-1}) compared with Doña María (30.94 Mg ha^{-1}) and Villaseca (33.89 Mg ha^{-1}) mirrors this pattern and illustrates the variability that plot-based LiDAR inventories need to capture in Mediterranean woody crops.

Compared with forest LiDAR benchmarks, such as those of Asner and Mascaro [1] and Silva et al. [2], who reported plot-scale AGB RMSE values of the order of 10–20% of the mean AGB from airborne LiDAR, the relative RMSE values obtained in this study (below 10% for most site and model combinations) indicate that the plot-scale AGB signal in orchards is relatively easy to capture with LiDAR, provided that species-specific allometries are applied. At the same time, the TreeQSM results obtained here contrast with those reported for terrestrial laser scanning in natural forests, where QSM has achieved R^2 values above 0.9 at the tree level [9]. In our woody-crop setting, only about 28% of the scanned trees produced usable QSM reconstructions and the site-level agreement with field inventory ranged from $R^2 = 0.42$ to 0.61, which reflects the more challenging acquisition geometry of orchards (narrow rows, pruned hedgerows, limited inter-row space for scanner trajectories) compared with open-grown forest trees. Finally, the competitive performance of the open PNOA/ALS dataset in this study is consistent with recent evidence that national LiDAR program can support large-scale AGB and carbon monitoring [17,18], and extends this evidence to Mediterranean woody crops, which have so far been under-represented in multi-platform LiDAR benchmarks.

5. Conclusions

This study demonstrates that multi-platform LiDAR, combined with a rigorous fixed-area field inventory and species-specific allometry, can support robust aboveground biomass (AGB), carbon, and CO_2e estimations in Mediterranean woody-crop systems. The field results revealed clear, statistically significant differences among Villaseca, Doña María, and IFAPA in key structural and carbon-related variables (e.g., tree density, biomass, and carbon), highlighting the importance of site conditions and management in shaping productivity and carbon storage. Across sites, the trunk diameter measured below the first bifurcation (D2r) behaved consistently and was strongly informative for overall tree development, supporting its use as a practical structural indicator. However, the orchard architecture, particularly hedgerow systems, suggests that LiDAR validation and inference are more defensible at the hedge-segment or plot level than at the individual-tree level.

In modeling, machine-learning approaches provide accurate plot-scale predictions, with XGBoost generally outperforming Random Forest and ensemble strategies, improving stability in several cases. Cross-sensor comparisons indicate that differences among LiDAR sources (e.g., ULS

 doi:10.20944/preprints202603.0280.v2

vs. ALS) can introduce systematic offsets, reinforcing the need for harmonization and calibration prior to pooling metrics or transferring models. TreeQSM-based quantitative structure modeling provided an informative, geometry-driven complement to area-based metrics but showed strong sensitivity to point-cloud quality and usability constraints, with performance varying by site and acquisition conditions. These limitations should be explicitly considered before operational deployment in orchard MRV. Overall, the workflow is transferable and can be replicated across agroforestry and woody-crop settings, provided that site-specific calibration, transparent validation design, and uncertainty reporting are implemented.

Supplementary Materials: The following supporting information can be downloaded at the website of this paper posted on Preprints.org. Table S1: UTM coordinates of the plot centroids (n = 58).

Author Contributions: Mateo Pastrana: Conceptualization, Methodology, Investigation, Formal analysis, Data curation, Visualization, Writing-original draft preparation, Writing-review and editing, Project administration. Mateo Pastrana led the overall research design, multi-platform LiDAR integration strategy, biomass and carbon modeling workflow, statistical analysis, and manuscript preparation. Cristina Velilla: Supervision, Conceptualization, Methodology, Writing-review and editing, Funding acquisition. Cristina Velilla provided doctoral supervision, high-level methodological guidance, and critical scientific revision of the manuscript. Sergio Molina: Methodology, Validation, Resources, Writing-review, and editing. Sergio Molina contributed expert input on ALS (PNOA) data processing standards, LiDAR validation strategies, and technical reviews of the derived products. Nelson Mattie: Conceptualization, Methodology, Investigation, Data curation, LiDAR data processing workflows, python programming, analytical development for biomass estimation, Formal analysis, Writing-review and editing. Alfonso Gomez: Conceptualization, Validation, Investigation. Alfonso Gomez contributed to the experimental design refinement, validation framework, and support in data interpretation. All authors have read and agreed to the published version of the manuscript.

Institutional Review Board Statement: Not applicable.

Informed Consent Statement: Not applicable.

Data Availability Statement: The processed point clouds, derived plot metrics, and analysis scripts were stored in a FAIR-aligned repository for the project. Data are available from the corresponding author upon reasonable request.

Acknowledgments: The ALS, ULS and MLS LiDAR datasets were acquired by Stereocarto Iberoamerica S.L. The authors acknowledge their technical support for the data acquisition. The company had no role in the study design, data analysis, or interpretation of results. The authors acknowledge IFAPA and the farm owners/managers (Doña María and Villaseca) for their access and logistical support. The authors have reviewed and edited the manuscript and take full responsibility for the content of this publication.

Conflicts of Interest: The authors declare no conflicts of interest.

Abbreviations

The following abbreviations are used in this manuscript:

AGB	Aboveground biomass
ALS	Airborne laser scanning
CHM	Canopy height model
CO2e	Carbon dioxide equivalent
DTM	Digital terrain model
GEDI	Global Ecosystem Dynamics Investigation
GNSS	Global Navigation Satellite System
IFAPA	Instituto de Investigación y Formación Agraria y Pesquera
IMU	Inertial measurement unit
MLS	Mobile laser scanning
MRV	Measurement–reporting–verification

Preprints.org (www.preprints.org) | NOT PEER-REVIEWED | Posted: 17 April 2026 doi:10.20944/preprints202603.0280.v2

PNOA National Aerial Orthophotography Plan (Spain)
ULS Unmanned laser scanning

Appendix A

Appendix A.1. Plot Centroid Coordinates

Table A1. UTM coordinates of plot centroids used for field inventory and LiDAR metric extraction.

Site	Plot	Easting	Northing
Doña María	1	338442.891	4177491.422
Doña María	2	338479.943	4177785.198
Doña María	3	338572.069	4178069.313
Doña María	4	338619.368	4178361.078
Doña María	5	338682.799	4178665.661
Doña María	6	338773.056	4178955.806
Doña María	7	338791.065	4179213.691
Doña María	8	338360.591	4178729.133
Doña María	9	338453.508	4179003.026
Doña María	10	338486.634	4179280.926
Doña María	11	338154.990	4177847.548
Doña María	12	338257.349	4178129.910
Doña María	13	338338.505	4178423.586
Doña María	14	337894.781	4177905.352
Doña María	15	337974.339	4178216.396
Doña María	16	338084.834	4178765.124
Doña María	17	338149.355	4179078.420
Doña María	18	337995.796	4178472.399
Villaseca	1	322488.703	4183949.082
Villaseca	2	322625.775	4184007.307
Villaseca	3	322734.451	4184066.151
Villaseca	4	322547.632	4184144.189
Villaseca	5	322673.036	4184206.089
Villaseca	6	322477.923	4184274.370
Villaseca	7	322407.454	4184406.609
Villaseca	8	322311.322	4184366.350
Villaseca	9	322605.783	4184333.879
Villaseca	10	322531.865	4184470.533
Villaseca	11	322525.107	4184568.767
Villaseca	12	322119.568	4184696.117
Villaseca	13	322787.640	4184703.639
Villaseca	14	322660.101	4184975.439
Villaseca	15	322943.758	4184435.829
Villaseca	16	322934.346	4184020.871
Villaseca	17	322693.976	4184269.419

doi:10.20944/preprints202603.0280.v2

Villaseca	18	322262.459	4184430.594
Villaseca	19	322625.344	4185315.724
Villaseca	20	322387.154	4184830.815
IFAPA	1	341170.695	4191371.022
IFAPA	2	341232.111	4191326.678
IFAPA	3	341205.203	4191261.724
IFAPA	4	341217.546	4191383.992
IFAPA	5	341191.305	4191315.048
IFAPA	6	341251.737	4191276.441
IFAPA	7	341314.457	4191314.919
IFAPA	8	341348.624	4191324.491
IFAPA	9	341387.266	4191334.331
IFAPA	10	341427.348	4191344.763
IFAPA	11	341464.099	4191353.589
IFAPA	12	341475.656	4191300.190
IFAPA	13	341435.214	4191289.675
IFAPA	14	341400.434	4191280.931
IFAPA	15	341361.690	4191270.790
IFAPA	16	341219.843	4191204.017
IFAPA	17	341265.128	4191226.961
IFAPA	18	341185.157	4191191.251
IFAPA	19	341144.323	4191175.878
IFAPA	20	341115.363	4191164.295

References

1. Asner, G.P.; Mascaro, J. Mapping tropical forest carbon: Calibrating plot estimates to a simple LiDAR metric. Remote Sens. Environ. 2014, 140, 614–624. https://doi.org/10.1016/j.rse.2013.09.023
2. Silva, C.A.; Hudak, A.T.; Vierling, L.A.; Klauberg, C.; Garcia, M.; Ferraz, A.; Keller, M.; Eitel, J.U.H.Saatchi, S. Impacts of airborne lidar pulse density on estimating biomass stocks and changes in a selectively logged tropical forest. Remote Sens. 2017, 9, 1068. https://doi.org/10.3390/rs9101068
3. Estornell, J.; Velázquez-Martí, B.; López-Cortés, I.; Salazar, D.; Fernández-Sarría, A. Estimation of wood volume and height of olive tree plantations using airborne discrete-return LiDAR data. GISci. Remote Sens. 2014, 51, 17–29. https://doi.org/10.1080/15481603.2014.883209
4. Velázquez-Martí, B.; López-Cortés, I.; Salazar-Hernández, D.M. Dendrometric analysis of olive trees for wood biomass quantification in Mediterranean orchards. Agrofor. Syst. 2014, 88, 755–765. https://doi.org/10.1007/s10457-014-9718-1
5. López-Bellido, P.J.; López-Bellido, R.J.; García-Morillo, J.; Fernández-García, P. Assessment of carbon sequestration and the carbon footprint in olive groves in Southern Spain. Int. J. Sustain. Dev. World Ecol. 2016, 23, 1–13. https://doi.org/10.1080/17583004.2016.1213126
6. Dubayah, R.; et al. The Global Ecosystem Dynamics Investigation: High-resolution laser ranging of the Earth's forests and topography. Remote Sens. Environ. 2020, 240, 111779. https://doi.org/10.1016/j.rse.2020.111779
7. Duncanson, L.; et al. Aboveground biomass density models for NASA's GEDI mission. Remote Sens. Environ. 2022, 270, 112845. https://doi.org/10.1016/j.rse.2021.112845

8. Khosravipour, A.; Skidmore, A.K.; Isenburg, M.; Wang, T.; Hussin, Y.A. Generating pit-free canopy height models from airborne lidar. Photogramm. Eng. Remote Sens. 2014, 80, 863–872. https://doi.org/10.14358/PERS.80.9.863
9. Kukko, A.; Kaartinen, H.; Hyyppä, J.; Chen, Y. Multiplatform mobile laser scanning: Usability and performance. Sensors 2012, 12, 11712–11733. https://doi.org/10.3390/s120911712
10. Breiman, L. Random forests. Mach. Learn. 2001, 45, 5–32. https://doi.org/10.1023/A:1010933404324
11. 11. Chen, T.; Guestrin, C. XGBoost: A scalable tree boosting system. In Proceedings of the 22nd ACM SIGKDD International Conference on Knowledge Discovery and Data Mining, San Francisco, CA, USA, 13–17 August 2016; pp. 785–794. https://doi.org/10.1145/2939672.2939785
12. IPCC. 2006 IPCC Guidelines for National Greenhouse Gas Inventories; Intergovernmental Panel on Climate Change: Geneva, Switzerland, 2006.
13. Kebede, B.; Soromessa, T. Allometric equations for aboveground biomass estimation of Olea europaea L. subsp. cuspidata in Mana Angetu Forest. Ecosyst. Health Sustain. 2018, 4, 1–12. https://doi.org/10.1080/20964129.2018.1433951
14. Henry, M.; Bombelli, A.; Trotta, C.; Alessandrini, A.; Birigazzi, L.; Sola, G.; Vieilledent, G.; Santenoise, P.; Longuetaud, F.; Valentini, R.; Picard, N.; Saint-André, L. GlobAllomeTree: International platform for tree allometric equations to support volume, biomass and carbon assessment. iForest 2013, 6, 326–330. https://doi.org/10.3832/ifor0901-006
15. Frank, B.; Mauro, F.; Allensworth, E. allometric: Structured Allometric Models for Trees. R package version 3.0.0, 2024. Available online: https://allometric.org/ (accessed on 26 February 2026).
16. Proietti, S.; et al. Carbon footprint of an olive tree grove. Appl. Energy 2014, 127, 115–124. https://doi.org/10.1016/j.apenergy.2014.04.019
17. Roussel, J.-R.; et al. lidR: An R package for analysis of airborne laser scanning (ALS) data. Remote Sens. Environ. 2020, 251, 112061. https://doi.org/10.1016/j.rse.2020.112061
18. LiDAR, Especificaciones técnicas. Plan Nacional de Ortofotografía Aérea (PNOA), Instituto Geográfico Nacional (IGN). Available online: https://pnoa.ign.es/pnoa-lidar/especificaciones-tecnicas (accessed on 26 February 2026).